Iranian Journal of Science and Technology, Transactions of Mechanical Engineering (2023) 47:959–968
https://doi.org/10.1007/s40997-022-00571-4

RESEARCH PAPER

Temporal–Spatial Analysis of the Flow Energy Loss in the Guide Vane and Circular Volute of Mixed-Flow Pump

Ran Tao[1,2] · Puxi Li[1] · Zhaoheng Lu[1] · Yanzhao Wu[1] · Di Zhu[3] · Kun Lin[4] · Ruofu Xiao[1,2]

Received: 17 May 2022 / Accepted: 29 November 2022 / Published online: 9 December 2022

Abstract

Vaned-voluted combined diffuser is usually applied to specific pump units requiring high stability. However, due to the non-uniform internal flow regime, the vaned-voluted diffuser usually leads to high flow energy loss. In this study, Detached Eddy Simulation with experimental validation was carried out to analyze the flow in a mixed-flow pump with radial guide vane and circular volute. The investigated point is the design flow rate point but falls out of the best efficiency range. Backflow, vortex, and flow non-uniform flow phenomena are observed. Swirling flow is also found in guide vane channels and mid-volute regions. The entropy production rate effectively indicates that the flow energy loss of the guide vane and volute is high. The temporal-spatial analysis with 5000 uniformly distributed points provides a good visualization of the temporally-averaged intensity and peak-peak value of flow energy loss and the spatial classification of a diffuser. The ratio between peak-peak value and averaged value has no absolute law, but is within a certain range. The combination of computational fluid dynamics, entropy production, and temporal-spatial analysis can help the optimization design.

Keywords Mixed-flow pump · Swirling flow · Circular volute · Entropy production · Flow energy loss

1 Introduction

The mixed flow pump is a common type of bladed pump, which is suitable for efficient transportation of liquid of medium or high head (Guan 2011). A diffuser of mixed flow pump includes vane type, volute type, and vaned-voluted combination type. The purpose of the diffuser is to collect the inflow from the impeller and transfer it to the next stage.

Circular volute is a common form of volute. Although it is not commonly used as the spiral volute, it also has some special applications. It is most commonly used in the rear of a segmented multistage centrifugal pump to reduce the geometric size (Baun et al. 2000). Circular volute is also commonly used as pumps to transport impurities, which can improve the passing ability of solid–liquid mixtures (Tao et al. 2019). Circular volute is also commonly used in nuclear main pumps. It is simple in structure, easy to manufacture and shape, strong in structural stability and low in surface roughness (Zhu et al. 2017). Since the cross-sectional area of the circular flow channel is equal everywhere, the liquid flow velocity is uneven everywhere compared with spiral channel (Stepanoff 1998). Therefore, it usually has a high flow energy loss (FEL). When the circular volute is used with the radial guide vane, the rotating fluid in the volute periodically collides with the fluid from the guide vane, which intensifies FEL (Long et al. 2017).

Many researchers have studied centrifugal pump or mixed flow pump with circular volute. Majidi and Siekmann (1998) studied the flow field in volute and circular casings interacting with a centrifugal impeller. It is found that the geometric curvature of volute causes pressure gradient and vortex at cross sections of the volute. Alemi et al. (2015) investigated the influence of volute curvature on performance of a low specific-speed centrifugal pump. The shape of circular volute has great influence on the head, efficiency and internal velocity distribution.

✉ Ruofu Xiao
xrf@cau.edu.cn

1 College of Water Resources and Civil Engineering, China Agricultural University, Beijing 100083, China

2 Beijing Engineering Research Center of Safety and Energy Saving Technology for Water Supply Network System, China Agricultural University, Beijing 100083, China

3 College of Engineering, China Agricultural University, Beijing 100083, China

4 Dongfang Electric Machinery Co. Ltd, Deyang 618000, China

Boehning et al. (2011) studied the radial force generated by the circular volute on the centrifugal pump impeller. It is found that the impeller radial force is closely related to the volute shape. Tao et al. (2018) found that the circular volute has a strong influence on the pressure pulsation characteristics of the pump. Generally, these results show that the advantages and disadvantages of circular volute are obvious and FEL caused by uneven flow is a major problem.

It is a consensus that the hydraulic loss of circular volute is greater than that of spiral volute. However, the specific location of its FEL is difficult to identify. The analysis of vortex distribution can reflect the flow complexity to a certain extent and point out the reasons for FEL (Trofimenko and Naida 2017; Li et al., 2021). However, the type of loss in fluid machinery is not only the loss caused by flow separation or other undesirable flow structures, but also friction loss of fluids flowing near walls (Lu et al. 2022). When the flow is smooth or complex, the friction loss near the wall may be large. In addition, vortical flow sometimes does not necessarily cause particularly large losses (Tao and wang 2021). For radial guide vanes, jet-wake and other flow structures at the tailing-edge of guide vane may complicate the situation (Wang et al. 2019).

Many researchers use the entropy production (EP) analysis to indicate the FEL. Esfahani et al. (2013) effectively applied EP to laminar duct flow. Kluxen et al. (2017) also studied the energy loss mechanisms of axial flow turbine stage based on the application of EP analysis. Li et al. (2016) investigated the EP in the pump-turbine model and visualized FEL well. Through the use of EP analysis, Soltanmohamadi and Lakzian (2016) completed the improvement of the Wells turbine unit design. Zeinalpour and Mazaheri (2015) optimized the turbine cascade by using algorithms to reduce the local EP strength. Zhao et al. (2019) applied EP analysis to the improvement of a centrifugal dredge pump under overload conditions. According to the second law of thermodynamics, this method reflects the FEL intensity through temperature variation and velocity variation, and has good accuracy. In particular, EP has significant advantages in spatial indication (Herwig and Kock 2007).

However, due to the periodic rotation of the impeller, the flow in fluid machinery evolves periodically. The advantage of EP in space must be coupled with time scale. This study is aimed at a mixed flow pump with vaned-voluted combined water chamber. On the basis of experiment verification and computational fluid dynamics (CFD), the temporal-spatial characteristics of FEL are clarified through high-spatial-resolution tracking. This study is of great significance to control the flow and eliminate the local excessive loss of the circular volute, and can guide the efficiency and stable operation of special pump types.

Table 1 Operation parameters of the pump unit

Parameter	Unit	Value
Design Flow Rate Q_D	[m^3/s]	0.2
Required Head H_{req}	[m]	3.5
Rotational Speed n	[rpm]	700
Specific Speed n_q	[–]	122.3

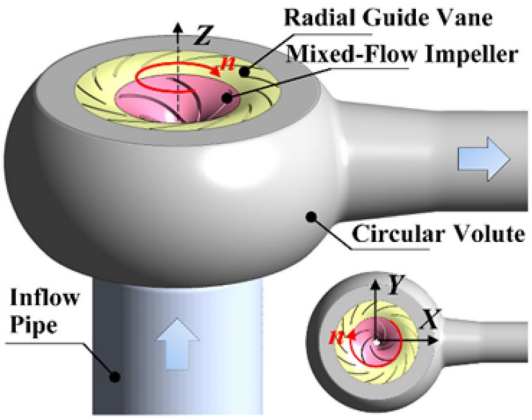

Fig. 1 Three-dimensional model of the fluid domain of pump

2 Research Objective

2.1 Parameters of Pump Unit

In this study, a mixed-flow pump unit is investigated. It has a 5-blade impeller with a diameter of 312 mm, a 13-blade radial guide vane and a circular volute. Table 1 lists the important operation parameters. The important operation parameters are listed in Table 1. The similarity parameter specific speed n_q can be calculated by the following formula:

$$n_q = n\frac{\sqrt{Q_D}}{H_{\mathrm{req}}^{3/4}} \tag{1}$$

In this case, n_q is about 122.3 and this pump can be classified into medium specific-speed pump.

2.2 Modeling of Fluid Domain

CFD is used to help the FEL analysis in this study. Therefore, it is necessary to model the fluid domain of the 4 main parts of the pump unit including inflow pipe, mixed-flow impeller, radial guide vane and circular volute. The model is shown in Fig. 1 with the indication of *X*-*Y*-*Z* coordinate directions and the rotation direction.

3 Computation Setup

3.1 Methodology

In this study, the zonal-hybrid Detached Eddy Simulation (DES) method is used to simulate the turbulent flow in the pump unit (Spalart 2009). DES model is very effective in dealing with large separated flows. It avoids the small-scale energetic vortex that needs to be solved in the near wall region of the large eddy simulation (LES) model, reduces the computation amount and has been verified by complex engineering examples. Shear stress transport-based DES (SST-DES) model is used in this study (Menter et al. 2003). When the grid size is smaller than the local eddy size, LES mode will be activated. Otherwise, the SST model based on Reynold-averaged mode will work. In this case, the automatic wall treatments were adopted to empirically model the near-wall flow. The total energy equation is also considered.

3.2 Grid Preparation

In this DES-based CFD case, grid is very important because it not only affects the simulation accuracy of pump performance but also affects the eddy resolution. Therefore, the grid in this study can be determined according to the following estimation methods (Pacot et al. 2016).

The highest speed position in this pump is the trailing-edge tip of the runner blade. The local tip velocity U_{tip} is about 11.43 m/s. The blade trailing-edge thickness l_{tbt} is about 0.011 m. The local Reynolds number Re_{loc} can be estimated by:

$$\text{Re}_{\text{loc}}=\rho\frac{U_{\text{tip}}l_{\text{tbt}}}{\mu} \tag{2}$$

where ρ is the density of fluid medium, μ is the dynamic viscosity of fluid medium. Re_{loc} is about 1.41×10^5. The viscous length scale L_{vic} is about 0.0013 mm. The 150–300 times of L_{vic}, which is about 0.2–0.4 mm, will be responsible to the production of turbulence kinetic energy in boundary layer.

Therefore, the grid element length in impeller, guide vane and the circular region of volute is controlled to be less than 1.0 mm, or even between 0.2 and 0.4 mm as far as possible. The value of y^+ in the near wall region especially on the blade is about 1.0. In the inflow pipe and the straight section of volute, where the eddy scale is usually large, the grid size is large. For the possible wall function, the y^+ value is less than 100. In this case, hexahedral elements are mainly used to reduce the calculation cost. In the case of complex geometry, tetrahedron elements are also used to enhance the grid quality (Fig. 2). The proportion of tetrahedral element is less than 5%. The details of the grid number and size are listed in Table 2 and the total node number of grid is 10561598, which exceeds the quantity level of common engineering calculation grid schemes.

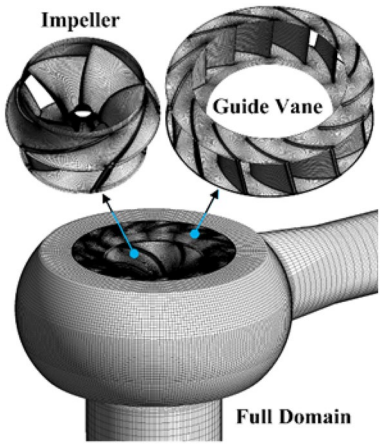

Fig. 2 Grid of the fluid domain of pump

Table 2 Grid number and size

Domain	Node Number	Mean Element Length
Inflow Pipe	1,113,186	5.0 [mm]
Impeller	3,861,330	0.3 [mm]
Guide Vane	4,292,922	0.4 [mm]
Volute	1,294,160	2.7 [mm]
Total	10,561,598	–

3.3 Setup of Simulation

In the setup of the CFD simulation, the fluid medium is set to 25 °C water. Cold water is used for analysis, which is convenient for model test. In practical engineering, it will be converted into hot water for application. The reference pressure is set to 1 Atm. In this case, the multiple reference frame model is used. The impeller domain is rotational at 700 rpm and the other domains are static. The inflow pipe inlet is a velocity type inlet with velocity magnitude and direction. The velocity magnitude depends on the flow rate. The volute outlet is a pressure outlet with a static pressure of 0 Pa. The transient rotor stator interfaces are given between each two domains. For the initial results, a maximum of 600 steps of steady state simulation was carried out. Impellers with more than 8 revolutions were transient simulated. Each impeller rotation gives 360 time steps, and each step gives 10 iterations. The convergence criteria are set as the root-mean-square residuals of continuity and momentum equation is less than 0.00001.

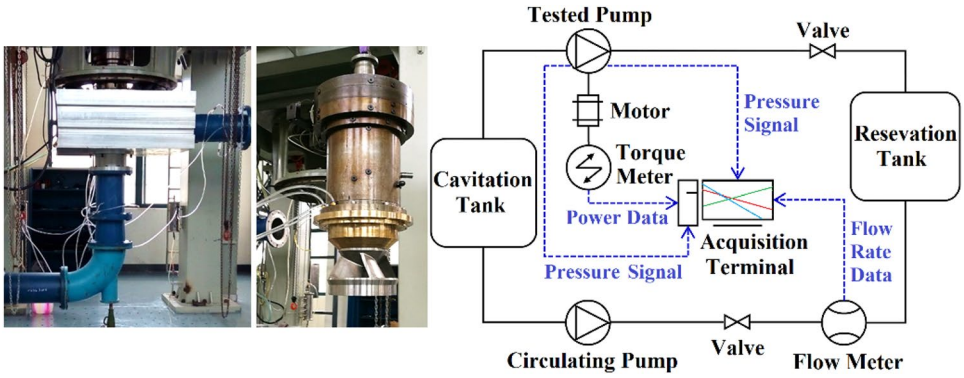

Fig. 3 Test rig and apparatus

4 Energy Performance Test

4.1 Test Rig and Method

The performance test of the mixed-flow pump unit is carried out on a closed hydraulic test rig as shown in Fig. 3. The tested pump is set between two water tanks and a circulating pump is used to supply water flow. The differential pressure transducer is used to measure the pressure signal at pump inlet p_{in} and outlet p_{out}. The pump head H can be calculated by:

$$H=\frac{p_{\text{out}}-p_{\text{in}}}{\rho g} \tag{3}$$

The electromagnetic flow meter is used to measure the flow rate data Q. The shaft torque M is measured by a torque meter set on the motor. The rotational speed n and the angular speed ω_n is measured by the encoder. The shaft power P is calculated by:

$$P=M\omega_n \tag{4}$$

Therefore, efficiency η is calculated by:

$$\eta=\frac{\rho g Q H}{P} \tag{5}$$

The Q-H and Q-η relationships can be used to evaluate the basic performance of pump and to be a validation of CFD result.

4.2 Test Results and Comparison

Figure 4 shows the Q-H and Q-η relationships of this mixed-flow pump based on experiment. In order to better compare with other pump units, the pump head H is normalized to H/H_{req} and the flow rate is normalized to Q/Q_D.

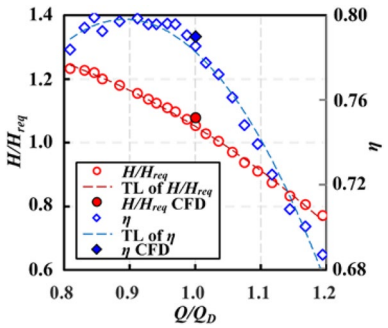

Fig. 4 Results of relative head H/H_{req} and efficiency η versus relative flow rate Q/Q_D with the trend lines (TL)

Table 3 Coefficients of trend lines

φ	C_0	C_1	C_2
H/H_{req}	3.44	4.91	−4.67
η	−0.26	2.36	−1.32

The trend line (TL) of Q/Q_D-H/H_{req} and Q/Q_D-η can find the variation tendencies. The quadratic polynomials can be used to express two TLs as:

$$\varphi=C_0+C_1q+C_2q^2 \tag{6}$$

where φ represents H/H_{req} or η, q represents Q/Q_D. C_1, C_2 and C_3 are coefficients as shown in Table 3.

As shown in the figure, the pump head decreases monotonically with the increase of flow rate. The pump efficiency presents a typical upper parabola. The best efficiency range (BER) is about $Q/Q_D=0.83-0.98$ and the best efficiency is about 80%. When $Q/Q_D=1.0$ (the design flow rate point), the efficiency BER decreases, indicating that FEL may increase. To understand the FEL, CFD simulation was conducted when $Q/Q_D=1.0$ and Fig. 4 also shows the H/H_{req} of CFD and CFD efficiency η_{CFD}. As known, the efficiency of CFD simulation only includes the hydraulic part η_h. The mechanical efficiency η_m and

volumetric efficiency η_v are excluded. Therefore, η_{CFD} in Fig. 4 is empirically corrected by (Guan 2011):

$$\eta_{\mathrm{CFD}} = \eta_h \cdot \eta_m \cdot \eta_v \tag{7}$$

where η_m and η_v are statistical data from handbooks. As compared, the predicted pump head and efficiency is very close to the experimental value. CFD simulated flow field can be used for the analysis at $Q/Q_D = 1.0$ in the next section.

5 Flow Field Distributions

For better analysis, as shown in Fig. 5, a 3-dimensional surface S_{plt} is extracted for plotting. It includes the mid-span of the impeller, the mid-span of the guide vane and a X–Y section of the circular part of the volute. Circumferential position θ is defined as indicated from $+X$ to $-Y$ to $-X$ to $+Y$. Its direction is the same as the impeller rotation direction. The radial position r is defined outwards from the impeller rotation center.

5.1 Pressure and Velocity

Pressure and velocity are the most basic parameters of flow field, which also reflect the change of energy. For better analysis, the pressure coefficient C_p and velocity coefficient C_v are defined as:

$$C_p = \frac{p - p_{\mathrm{in}}}{\rho g H} \tag{8}$$

$$C_v = \frac{v}{U_{\mathrm{tip}}} \tag{9}$$

Two positions are highlighted in Fig. 6 with the indication of 'a' and 'b'. The 'a' position is approximately between $\theta = 30$ degrees and $\theta = 120$ degrees. The flows in different directions collide with each other here, forming undesirable flow structures such as local backflow and vortex. The 'b' position is approximately between $\theta = 135$ degrees and $\theta = 210$ degrees. The flow is squeezed at this position, and the streamline is significantly bent.

In order to analyze the flow uniformity in volute, Fig. 7 shows the circumferential velocity distribution along radial direction. A total of 7 positions (one line every 45 degrees) are analyzed as shown in this figure. C_{vt} in Fig. 7 is the circumferential component of C_v. The zero-velocity lines are shifted for a better view. Since the increasing direction of θ is consistent with the impeller flow-driving direction, it indicates that there is local backflow or vortex

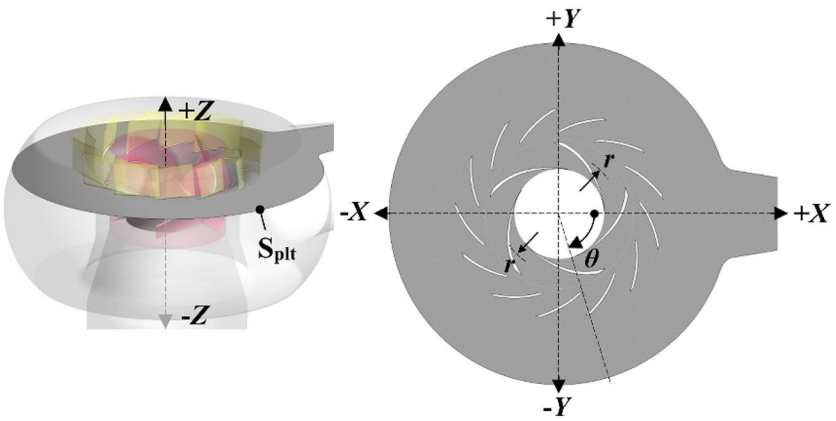

Fig. 5 Surface and definitions for plot and analysis

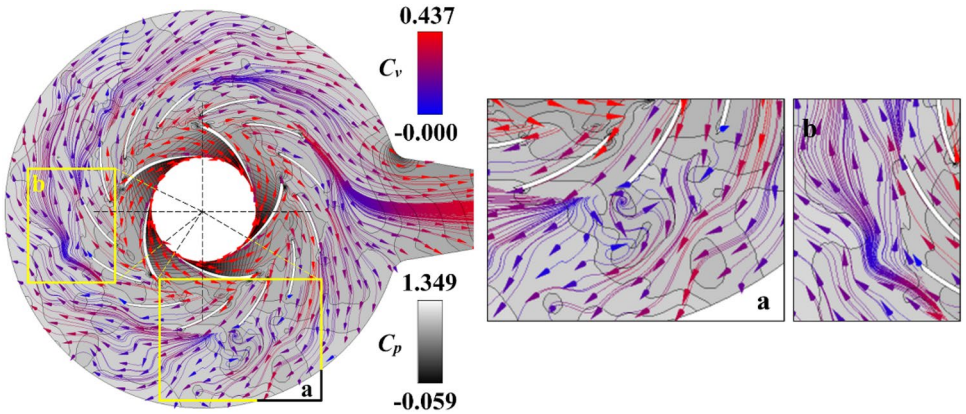

Fig. 6 C_p contour and C_v vectors with streamlines

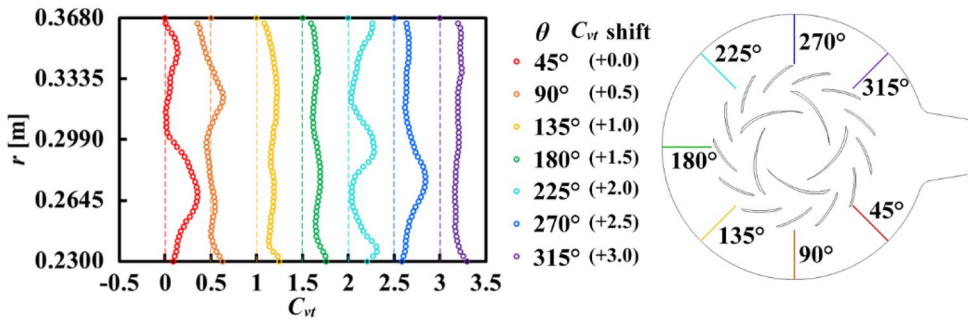

Fig. 7 Distribution of velocity in the circular part of volute

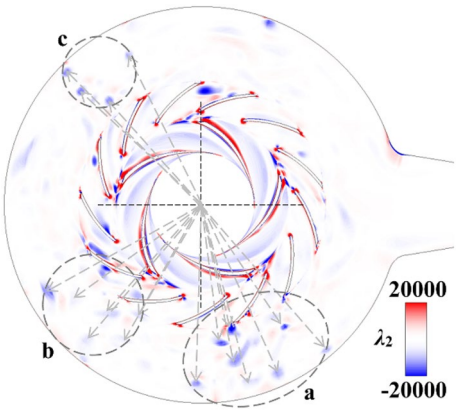

Fig. 8 Contour of swirling flow identifier λ_2

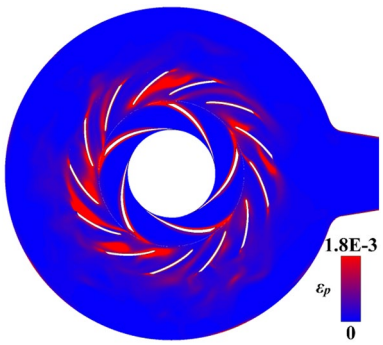

Fig. 9 Contour of the dimensionless local entropy production rate ε_p

if the velocity value approaches or crosses the zero lines to its left.

As shown in Fig. 7, C_{vt} in the region of $r=0.3-0.32$ m is close to the zero line of $\theta=45$ degrees. It indicates a local back flow or vortex which does not follow the impeller flow driving direction. For $\theta=90$ degrees, C_{vt} has multiple intersections with the shifted zero line. The local backflow is very strong, and the velocity is obviously non-uniform. For $\theta=225$ degrees, C_{vt} is close to the shifted zero line at $r=0.27$ m and $r=0.32$ m. This is also a typical case of local backflow. For the other θ situations in this case, C_{vt} is always obviously greater than 0 and the velocity uniformities are very good.

5.2 Identification of Swirling Flow

Based on the analysis of pressure and velocity, Fig. 8 shows the identification of swirling flow by using λ_2 contour. Positive and negative sites have strong swirling flow in different directions. In guide vane, strong λ_2 can be found in almost every blade channel. Near guide vane blade leading-edge and trailing-edge, strong λ_2 is mainly positive. In the middle of channels, strong λ_2 is mainly negative. However, from the streamline view, the flow in the guide vane channels is smooth.

In volute, there are three main regions 'a', 'b', and 'c' with multiple strong negative λ_2 cores. Region 'a' almost overlaps the backflow region 'a' in Fig. 6. The circumferential position is between $\theta=45$ degrees and $\theta=90$ degrees. Region 'b' locates upstream of the flow-squeezing region 'b' in Fig. 6. The circumferential position is between $\theta=120$ degrees and $\theta=150$ degrees. Region 'c' locates between $\theta=225$ degrees and $\theta=240$ degrees but the streamlines in Fig. 6 are somehow smooth. A strong positive λ_2 region can be found in the throat region between the circular part and the straight part.

5.3 Flow Energy Loss

Based on SST-DES, it is able to evaluate the FEL by plotting the local entropy production rate E_{pro} induced by velocity pulsation as (Herwig and Kock 2007; Zhou et al. 2018):

$$E_{\text{pro}} = \beta \frac{\rho \omega k}{T} \tag{10}$$

where β is the constant in turbulence model of 0.09. k is the turbulence kinetic energy, ω is the turbulent eddy frequency, T is temperature. The dimensionless local entropy production rate ε_p is used here by:

$$\varepsilon_p = \frac{E_{\text{pro}}}{\rho\sqrt{Hg^3}} \tag{11}$$

As observed in Fig. 9, the distribution of ε_p has a characteristic that it is very strong in the guide vane channel and slightly weaker in the volute. Relatively strong ε_p in volute is located in the 'a' region in Figs. 6 and 8. This indicates that FEL is closely related to whether the flow pattern is good or not.

It is necessary to carry out the volume integration on ε_p in each domain as shown in Fig. 10. The inflow pipe only account for 1.42% of the total FEL. Impeller takes up 14.36% of the total FEL. As shown in Fig. 9, FEL is mainly located at the suction side of the blade and the wake area at the trailing edge of the blade. The guide accounts for 28.15% of the total FEL as indicated by the strong ε_p in the blade channels. Volute accounts for 56.07% of the total FEL, more than the summary of other domains. Although the ε_p intensity shown in the contour is not as high as that of the guide vane, the circular volute has a larger volume and more loss accumulation, which is the most dominant in all domains.

6 Temporal-Spatial Analysis

6.1 Tracking Network of Flow Energy Loss

Based on the analysis above, guide vane and volute are the two main sources of FEL. Therefore, as shown in Fig. 11, a total of 5000 monitoring points are uniformly set in the guide vane part and volute part of S_{plt} to build the spatial tracking network (Jin et al. 2021) in stators. The spatial distribution of temporally-averaged intensity, peak-peak value and the spatial classification can be analyzed in detail in the following sections.

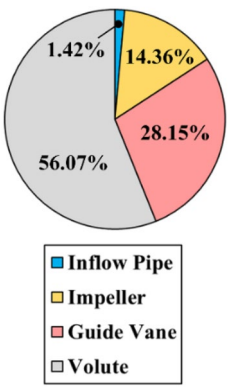

Fig. 10 Proportion of the dimensionless local entropy production rate ε_p in different domains

6.2 Temporally-Averaged Intensity

The temporally-averaged intensity I_{et} is analyzed within the last two impeller revolutions. It is defined as the average value of ε_p within the monitoring period:

$$I_{et} = \overline{\varepsilon_p} \tag{12}$$

This parameter can reflect the continuous intensity of FEL in a certain region, that is, it shows the spatial position where FEL is always strong.

Figure 12 shows the I_{et} contour on the guide vane part and volute part of S_{plt}. I_{et} is very strong in guide vane channels and in a local region in the circular part of volute. The local region in volute is the backflow region 'a' in Fig. 6. This indicates that undesirable flow pattern and FEL persist in this region. In addition, I_{et} is very strong in the near-wall region of volute.

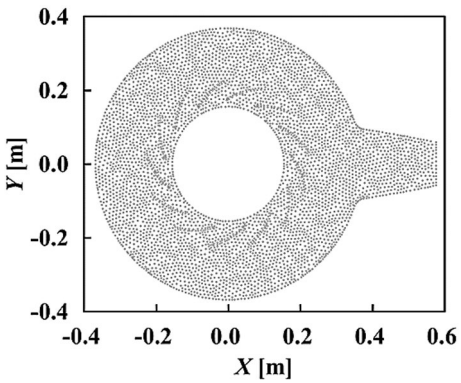

Fig. 11 Monitoring points set on the guide vane and volute part of S_{plt}

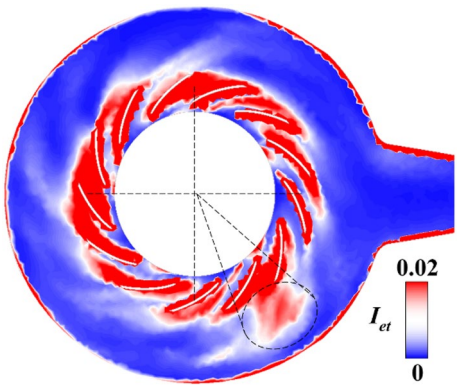

Fig. 12 Contour of the temporally-averaged intensity I_{et} in stators

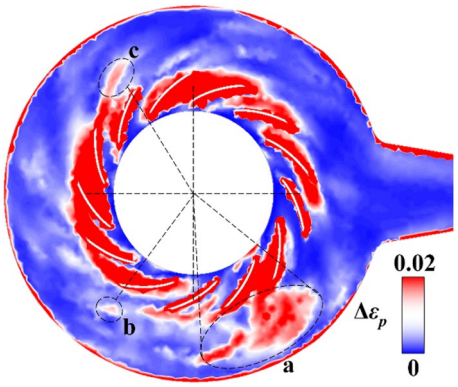

Fig. 13 Contour of the peak-peak value $\Delta\varepsilon_p$ in stators

6.3 Peak-Peak Value

The peak-peak value of ε_p can reflect the pulsation of FEL. It can be denoted as $\Delta\varepsilon_p$ which is the maximum-minimum difference:

$$\Delta\varepsilon_p = \varepsilon_{\text{pmax}} - \varepsilon_{\text{pmin}} \tag{12}$$

Figure 13 shows the contour of $\Delta\varepsilon_p$ on the guide vane part and volute part of S_{plt}. It is similar to the I_{et} contour in the guide vane region where FEL pulsation is very strong. However, it is more complex in the circular section of volute. As indicated by the high-intensity 'a', 'b', 'c' regions and other moderate-intensity regions, the pulsation of FEL is much more obvious than its average state. It also shows the complexity of the flow variation in the circular volute.

6.4 Spatial Classification

Based on the peak-peak value $\Delta\varepsilon_p$ on all the 5000 points, it is able to have a spatial classification of FEL. Figure 14 shows the $\Delta\varepsilon_p$ of all the 5000 points in a 3D view with different radial directions r and circumferential direction θ. It seems that $\Delta\varepsilon_p$ at different radial positions has great differences. A projective view of r-$\Delta\varepsilon_p$ relationship is drawn and it clearly indicates 4 regions. The region where $\Delta\varepsilon_p$ is very strong is the guide vane. The local $\Delta\varepsilon_p$ can be up to 0.35. According to the color legend, all the circumferential positions have large values. With the increase of r, $\Delta\varepsilon_p$ becomes very low in the mid-volute region and suddenly rises up to about 0.05 on the wall of the circular part of volute. As the radius continues to increase, there are few points that can be found with $\Delta\varepsilon_p$ of 0.02 – 0.05. This is the wall region at the throat part of volute where the θ value is approximately 0 degree and 360 degrees.

Because the characteristics of FEL in different circumferential positions are not clear enough, the circumferential position is divided into 8 equal areas for better comparative analysis, as shown in Fig. 15. For temporally-averaged

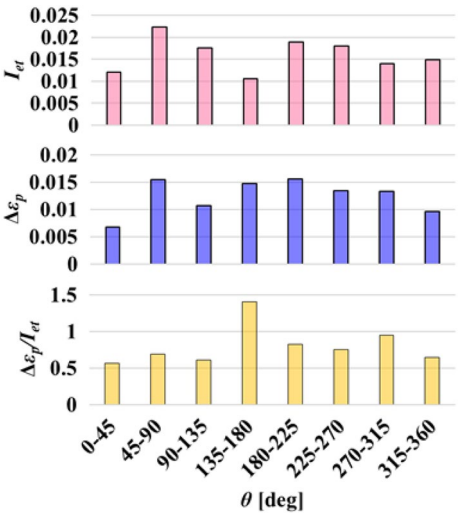

Fig. 15 Average value of I_{et} and $\Delta\varepsilon_p$ within different θ ranges

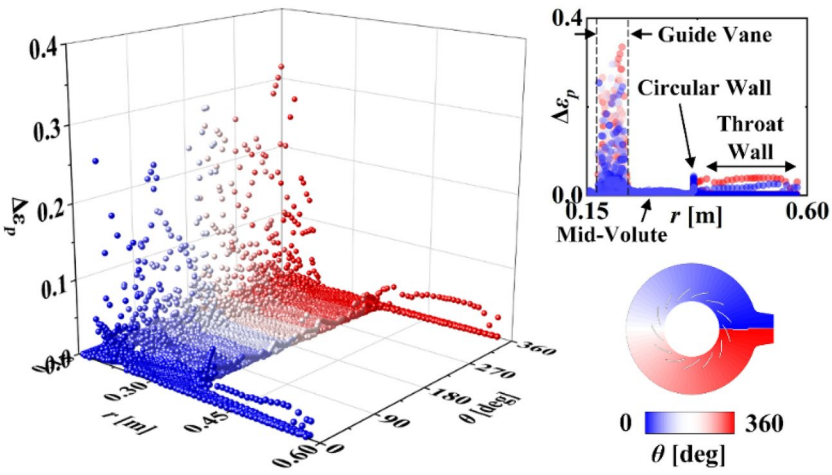

Fig. 14 Spatial classification of FEL based on $\Delta\varepsilon_p$

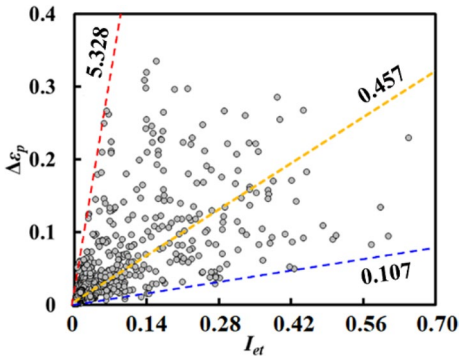

Fig. 16 The relationship between I_{et} and $\Delta\varepsilon_p$ with slopes

intensity I_{et}, the range of $\theta=45-90$ degrees is obviously stronger because of the backflow region in volute. The range of $\theta=270-315$ degrees, $\theta=315-360$ degrees and $\theta=0-45$ degrees have lower I_{et} because flow regime is smoother. For peak-peak value $\Delta\varepsilon_p$, the ranges of $\theta=45-90$ degrees and $\theta=180-225$ degrees are stronger than the other regions which indicates a local strong flow pulsation. The ranges of $\theta=315-360$ degrees and $\theta=0-45$ degrees have lower $\Delta\varepsilon_p$ due to smooth local flow.

There is a special θ range of 135 – 180 degrees that I_{et} is weak and $\Delta\varepsilon_p$ is strong. The local FEL is not high, but the pulsation is obvious. In Fig. 14, the $\Delta\varepsilon_p/I_{et}$ value is obviously larger than the others. Therefore, it is necessary to analyze the relationship between I_{et} and $\Delta\varepsilon_p$ as in Fig. 16. For different spatial positions, the relationship between I_{et} and $\Delta\varepsilon_p$ is very different. The mean slope of the 5000 points is about 5.328. The maximum slope is about 0.457 and the minimum slope is about 0.107. The samples with larger slope means that the variation of flow energy loss is relatively strong. This is related to the rapid change of local flow, but does not represent the level of loss. These regions are most closely related to the varying vortex flow. The samples with a small slope mean that the absolute value of flow energy loss is very high, but the change range is small. The flow in these regions is stable, and the loss mainly exists in the form of interaction between flow and wall.

7 Conclusions

This study mainly focuses on the flow energy loss in a mixed-flow pump unit and makes the temporal-spatial analysis of the guide vane and volute. Conclusions are as follows:

(1) As a typical bladed pump, the flow head relationship of this unit presents a typical monotonic decline, and the flow efficiency relationship is an upper parabola. The efficiency of the design flow rate point is not within the best efficiency range, and the optimal efficiency of the unit is also at 80% level. This is related to the setting of the combination of radial guide vane and circular volute.

(2) Vortex and backflow are mainly distributed in the circular section of volute, especially in the range of $\theta=45-90$ degrees. In the guide vane, the flow pattern is good. However, the FEL reflected by entropy production ε_p shows that the losses are large in both guide vane and volute. The local ε_p strength in guide vane is high, and the overall integral ε_p in volute is the largest. The results show that there is a close relationship between FEL and swirling flow.

(3) The temporal-spatial characteristics of FEL can clarify the distribution of temporally-averaged intensity I_{et} and peak-peak value $\Delta\varepsilon_p$. It is found that both I_{et} and $\Delta\varepsilon_p$ are large in guide vane. $\Delta\varepsilon_p$ is large in the backflow and vortex region, near wall region and throat wall region of volute. The $\Delta\varepsilon_p/I_{et}$ ratio indicates that there is a certain range but no absolute law between the two parameters. The slope is between 5.328 and 0.457, with a 5000 points' average value of 0.107.

In general, the temporal-spatial analysis based on entropy production will help to indicate the high FEL regions. This is of great significance for the optimization and improvement of circular volute and radial guide vane in future works.

Acknowledgements The authors would like to acknowledge the financial support of National Natural Science Foundation of China. This study is funded by National Natural Science Foundation of China grant number 52079142.

Funding National Natural Science Foundation of China, 52079142, Ruofu Xiao

References

Alemi H, Nourbakhsh SA, Raisee M, Najafi AF (2015) Effects of volute curvature on performance of a low specific-speed centrifugal pump at design and off-design conditions. J Turbomach 137(4):041009

Baun DO, Ko L, Flack RD (2000) Effect of relative impeller-to-volute position on hydraulic efficiency and static radial force distribution in a circular volute centrifugal pump. J Fluids Eng 122(3):598–605

Esfahani JA, Modirkhazeni M, Mohammadi S (2013) Accuracy analysis of predicted velocity profiles of laminar duct flow with entropy generation method. Appl Math Mech 34:971–984

Guan X (2011) Modern pumps theory and design. China Astronautic Publishing House, Beijing

Herwig H, Kock F (2007) Direct and indirect methods of calculating entropy generation rates in turbulent convective heat transfer problems. Heat Mass Transf 43(3):207–215

Jin F, Tao R, Lu Z, Xiao R (2021) A spatially distributed network for tracking the pulsation signal of flow field based on CFD simulation: method and a case study. Fractal Fract 5:181

Kluxen R, Behre S, Jeschke P, Guendogdu Y (2017) Loss mechanisms of interplatform steps in a 15-stage axial flow turbine. J Turbomach 139:031007

Li D, Gong R, Wang H, Xiang G, Wei X, Qin D (2016) Entropy production analysis for hump characteristics of a pump turbine model. Chin J Mech Eng 29:803–812

Li W, Ji L, Li E, Shi W, Agarwal R, Zhou L (2021) Numerical investigation of energy loss mechanism of mixed-flow pump under stall condition. Renew Energy 167:740–760

Long Y, Wang D, Yin J, Hu Y, Ran H (2017) Numerical investigation on the unsteady characteristics of reactor coolant pumps with non-uniform inflow. Nucl Eng Des 320:65–76

Lu Z, Xiao R, Tao R, Li P, Liu W (2022) Influence of guide vane profile on the flow energy dissipation in a reversible pump-turbine at pump mode. J Energy Storage 49:104161

Majidi K, Siekmann HE (1998) Numerical calculation of secondary flow in pump volute and circular casings using 3D viscous flow techniques. Int J Rotating Mach 6:162359

Menter F, Kuntz M, Langtry R (2003) Ten years of industrial experience with the SST turbulence model. Turbul Heat Mass Transf 4:625–632

Pacot O, Kato C, Guo Y, Yamade Y (2016) Computations of cavitating vortex rope by using LES. Seisan Kenkyu 68(1):63–68

Soltanmohamadi R, Lakzian E (2016) Improved design of wells turbine for wave energy conversion using entropy generation. Meccanica 51:1713–1722

Spalart PR (2009) Detached-eddy simulation. Annu Rev Fluid Mech 41:181–202

Stepanoff AJ (1998) Centrifugal and axial flow pumps: theory, design, and application. Springer, Vienna

Tao R, Wang Z (2021) Comparative numerical studies for the flow energy dissipation features in a pump-turbine in pump mode and turbine mode. J Energy Storage 41:102835

Tao R, Xiao R, Liu W (2018) Investigation of the flow characteristics in a main nuclear power plant pump with eccentric impeller. Nucl Eng Des 327:70–81

Tao Y, Yuan S, Liu J, Zhang F (2019) Influence of cross-sectional flow area of annular volute casing on transient characteristics of ceramic centrifugal pump. Chin J Mech Eng 32:161–173

Trofimenko PE, Naida MB (2017) Analysis of experimental studies of energy characteristics of a pump with centrifugal vortex stage. Int Appl Mech 53(1):116–120

Wang X, An C, Fu Q, Zhu R, Lu Y, Cai Z, Jiang X (2019) Grey relational analysis and optimization of guide vane for reactor coolant pump in the coasting transient process. Ann Nucl Energy 133:431–440

Zeinalpour M, Mazaheri K (2015) Entropy minimization in turbine cascade using continuous adjoint formulation. Eng Optim 48:213–230

Zhao X, Wang Z, Xiao Y, Luo Y (2019) Thermodynamic analysis of energy dissipation and unsteady flow characteristic in a centrifugal dredge pump under over-load conditions. Proc Inst Mech Eng C J Mech Eng Sci 233(13):4742–4753

Zhou Q, Xia L, Zhang C (2018) Internal mechanism and improvement criteria for the runaway oscillation stability of a pump-turbine. Appl Sci 8(11):2193

Zhu R, Liu Y, Wang X, Fu Q, Yang A, Long Y (2017) The research on AP1000 nuclear main pumps' complete characteristics and the normalization method. Ann Nucl Energy 99:1–8